Contents list available at CBIORE journal website

International Journal of Renewable Energy Development

Journal homepage: https://ijred.cbiore.id

Research Article

Methyl ester production from high free fatty acid content with Ce/Zeolite bifunctional catalyst

Aisyah Sabrina Nurul Syahidah[a*], Dinanti Putrisia Wilujeng[a], W. Widayat[a], H. Hadiyanto[a], S. Sulardjaka[b], Noorzita Ngadi[c]

[a]*Department of Chemical Engineering, Faculty of Engineering, Diponegoro University, Jl. Prof. Soedharto, S.H. Tembalang Semarang 50275, Central Java, Indonesia*

[b]*Department of Mechanical Engineering, Faculty of Engineering, Diponegoro University, Jl. Prof. Soedharto, S.H. Tembalang Semarang 50275, Central Java, Indonesia*

[c]*Faculty of Chemical and Energy Engineering, Universiti Teknologi Malaysia, 81310 UTM Johor Bahru, Johor, Malaysia*

Abstract. The production of methyl esters from high free fatty acid (FFA) feedstock remains a critical challenge in biodiesel processing, particularly when using Palm Acid Oil–waste cooking oil (PAO–WCO) with an initial FFA content of 53.21%. Such high FFA content significantly reduces reaction efficiency and necessitates a conventional two-step process involving esterification to lower the FFA level followed by transesterification to convert triglycerides into methyl esters. This multistep approach limits process efficiency and increases operational complexity for high-FFA feedstock. This study investigates the use of a bifunctional Ce/Zeolite catalyst to enable simultaneous esterification and transesterification in a single-step process for high FFA content oil. The zeolite support was synthesized from geothermal waste, and cerium was incorporated via impregnation. The catalyst was characterized using SEM–EDX, X-ray diffraction (XRD), and Brunauer–Emmett–Teller (BET) surface area analyses. The reaction was conducted under various operating conditions, including different temperatures and catalyst loadings. The Ce/Zeolite catalyst exhibited effective bifunctional activity, enhancing the simultaneous conversion of FFAs and triglycerides in high FFA content feedstock. The optimum conditions were a methanol-to-oil molar ratio of 12:1, 4 wt% catalyst loading, and a reaction temperature of 50 °C for 180 min. Under these conditions, FAME concentration of 91.5% was obtained, with FFA conversion of 25.31% (reduction of 13.47% FFAs from initial 53.21%) achieved in a single-step transesterification process. These results demonstrate that Ce/Zeolite is a promising bifunctional catalyst for the efficient processing of high FFA content oil, offering a simplified and more sustainable pathway for industrial biodiesel production.

Keywords: bifunctional catalyst; Ce/Zeolite; methyl ester; high free fatty acid; esterification; transesterification

Received: 4th Nov 2025; Revised: 16th Feb 2026; Accepted: 10th March 2026 ; Available online: 15th March 2026

1. Introduction

Global energy demand continues to increase, particularly in developing countries, driven by rapid industrialization, population growth, and continued reliance on fossil fuels. This dependence contributes significantly to greenhouse gas emissions and environmental degradation. In response to the global energy crisis, biodiesel—commonly referred to as Fatty Acid Methyl Ester (FAME)—has gained considerable attention as a renewable and sustainable alternative to fossil-based fuels (Yaakouby *et al.*, 2025). Biodiesel is produced through the transesterification of biomass-derived lipids, including vegetable oils, animal fats, and waste oils. Its application has been shown to substantially reduce emissions of CO, NOx, SOx, hydrocarbons, and particulate matter, thereby mitigating smog formation, acid rain, and global warming (Widayat *et al.*, 2024).

Among the available feedstocks, Palm Acid Oil (PAO) and Waste Cooking Oil (WCO) are abundant and economically attractive resources in Indonesia, making them promising raw materials for FAME production. PAO is a by-product of palm oil refining derived from Palm Oil Mill Effluent (POME), which contains approximately 3–5% PAO and 95–97% water. The Free Fatty Acid (FFA) content of PAO ranges from 27.6% to 81.2%, depending on feedstock characteristics and the alkaline refining process (Rachmadona *et al.*, 2022). However, the elevated FFA content presents significant challenges in conventional base-catalyzed transesterification due to soap formation, reduced catalytic efficiency, and difficulties in reagent optimization (Hadiyanto *et al* 2016). Direct blending of PAO with diesel has been proposed as a simpler alternative; however, this approach does not adequately address fuel quality and conversion efficiency.

Production of FAME from high-FFA oils typically requires a two-step process consisting of acid-catalyzed esterification to reduce FFA levels, followed by base-catalyzed transesterification of triglycerides. In this context, heterogeneous catalysts are widely employed to enhance biodiesel synthesis efficiency (Falowo *et al.*, 2024). In the present study, the high FFA content of PAO was adjusted by blending it with WCO, which possesses lower FFA levels. The

* Corresponding author
Email: aisyahsabrinasyahidah06@gmail.com (A. S. N. Syahidah)

https://doi.org/10.61435/ijred.2026.61945
ISSN: 2252-4940/© 2026.The Author(s). Published by CBIORE

oils were mixed at a volumetric ratio of 2:1 (20 mL PAO and 10 mL WCO), resulting in an initial FFA content of 53.21%, and subsequently preheated at 100 °C for 1 h. Although effective, this two-step approach increases processing time and operational costs. A promising alternative is the use of bifunctional heterogeneous catalysts capable of simultaneously catalyzing esterification and transesterification reactions (Gonzaga *et al*., 2021). Various bifunctional systems, including Zeolite/MOF and Zeolite-A/Biochar composites, have demonstrated high product yields, excellent recyclability, and strong substrate selectivity (Zhu *et al*., 2014). The Zeolite-A/Biochar (Z-A/BC) composite, for instance, has been reported as an environmentally friendly bifunctional catalyst with notable recyclability and dual selectivity toward FFA esterification and triglyceride transesterification, thereby minimizing side reactions and waste generation (Abdullah *et al*., 2021).

This study focuses on the synthesis of cerium (Ce)-modified beta zeolite derived from geothermal waste. Incorporation of Ce into the zeolite framework modifies the distribution of acidic sites within the micropores and on the external surface, thereby enhancing catalyst stability and reusability. Cerium exhibits high oxygen storage capacity and moderate basicity, while geothermal waste-derived zeolite provides high surface area and strong thermal stability, making it an effective and sustainable catalyst support (Widayat *et al*., 2019). The Ce/Zeolite catalyst exhibits bifunctional activity through Brønsted and Lewis acid sites originating from the zeolite framework and basic or oxidative sites associated with CeO_2. This dual functionality enables simultaneous esterification of FFAs at acid sites and transesterification of triglycerides at basic or methoxide-forming sites, facilitating one-step biodiesel synthesis. Bifunctional catalysts therefore improve process efficiency and reduce production costs (Ramli *et al*., 2017). The basic sites of CeO_2 generate methoxide ions (CH_3O^-) via proton abstraction from methanol, which subsequently attack the carbonyl groups of triglycerides to initiate transesterification. The presence of oxygen vacancies and strong basicity further enhances methoxide formation (Kingkam *et al*., 2024). Meanwhile, Brønsted and Lewis acid sites protonate the carbonyl groups of FFAs, facilitating ester formation without soap generation—a common limitation in homogeneous base-catalyzed systems (Fattahi *et al*., 2019)

Beta zeolite is a high-silica, large-pore material characterized by excellent chemical and thermal stability. Its hydrophobicity at high Si/Al ratios and the presence of surface silanol groups make it a suitable support for metal oxides. Modified beta zeolite has demonstrated improved stability and higher conversion efficiency in methyl ester synthesis due to the increased availability of external Brønsted acid sites (Fattahi *et al*., 2019). Additionally, CeO_2 provides strong basicity that enhances alcohol activation, particularly for methanol and ethanol, thereby improving transesterification efficiency (Jumari & Purwanto, 2013).

Therefore, this research develops a bifunctional Ce/Zeolite catalyst derived from geothermal waste and evaluates its performance in converting PAO and WCO into biodiesel via a single-step esterification–transesterification process. Process optimization was conducted using Response Surface Methodology (RSM) to maximize biodiesel yield and efficiency. The catalysts were characterized using SEM–EDX, XRD, and BET analyses. Furthermore, the effects of reaction temperature and catalyst concentration on FFA conversion, FAME yield, and triglyceride conversion were systematically investigated.

2. Materials and Method

The integrated experimental workflow implemented in this study, commencing with geothermal waste pretreatment and zeolite synthesis, followed by cerium impregnation to produce the bifunctional Ce/Zeolite catalyst, and culminating in the simultaneous esterification–transesterification of the PAO–WCO feedstock. The overall methodological sequence and process configuration are schematically presented in Figure 1. The schematic representation clarifies the sequential linkage between catalyst preparation, physicochemical characterization, and catalytic reaction stages that ultimately lead to methyl ester production and subsequent performance evaluation.

2.1 Materials

The primary feedstocks employed in this study were Palm Acid Oil (PAO) and Waste Cooking Oil (WCO). PAO was obtained as a by-product of palm oil refining, whereas WCO was collected from household cooking waste. A fixed volumetric ratio of 2:1 (PAO:WCO) was applied, resulting in an initial Free Fatty Acid (FFA) content of 53.21%. Cerium nitrate hexahydrate ($Ce(NO_3)_3{\cdot}6H_2O$, 99%) was used as the cerium precursor for the bifunctional catalyst. Geothermal solid waste obtained from PT. Geo Dipa Energi, Dieng, Wonosobo, served as the silica–alumina source for zeolite synthesis. Analytical-grade reagents, including hydrochloric acid (HCl, 37%), sodium hydroxide (NaOH), aluminum sulfate ($Al(SO_4)_3{\cdot}18H_2O$, 98%), sulfuric acid (H_2SO_4, 98%), and methanol, were utilized for catalyst preparation and biodiesel production. Distilled water was used throughout all experimental procedures.

2.2 Zeolite Synthesis from Geothermal Waste

Geothermal solid waste was first ground and sieved through a 125 µm mesh. Subsequently, 500 g of the obtained powder was treated with 2 L of 0.6% HCl under stirring at 100 rpm for 30 min to remove impurities. The suspension was filtered, washed

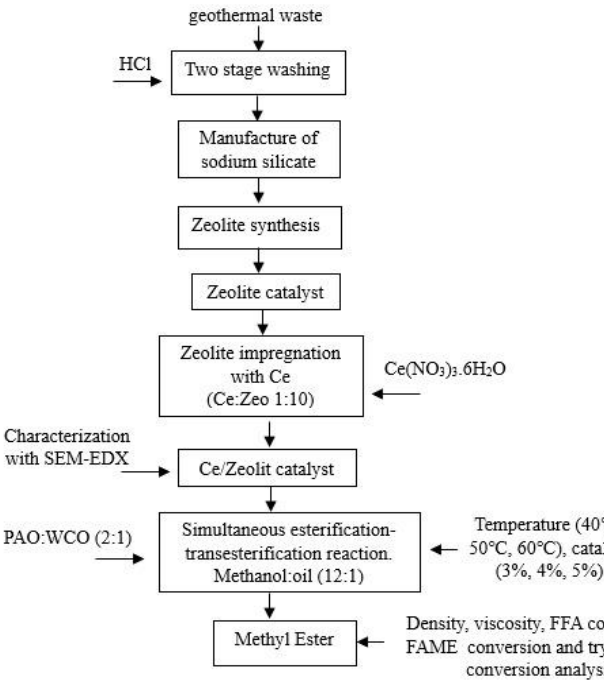

Fig 1. Schematic representation of the integrated experimental workflow

with distilled water until neutral pH was achieved, dried at 200°C for 1 h, and calcined at 850°C for 3 h. For sodium silicate preparation, 250 g of the calcined material was dissolved in 1000 mL of 2 N NaOH and stirred at 30°C and 300 rpm for 2 h. The synthesis gel was prepared by dissolving 26.7 g of $Al(SO_4)_3 \cdot 18H_2O$ in a mixture of 31 mL H_2SO_4 (98%) and 135 mL distilled water, followed by the addition of 250 mL sodium silicate solution and 140 mL of 10 N NaOH. The resulting mixture was stirred for 6 h to ensure homogeneity and subsequently subjected to hydrothermal crystallization at 150°C for 5 h in an autoclave. After crystallization, the solid product was washed repeatedly until neutral pH, dried at 105°C for 6 h, ground into fine powder, and calcined at 550°C for 6 h with a heating rate of 5°C min^{-1}. The synthesized zeolite was characterized using X-ray diffraction (XRD) and Brunauer–Emmett–Teller (BET) surface area analysis to evaluate its crystalline structure and textural properties.

2.3 Preparation and Characterization of Ce/Zeolite Catalyst

The Ce/Zeolite catalyst was prepared following the impregnation method reported by Akream *et al.* (2024). Briefly, 50 g of zeolite was impregnated with x.50 g of cerium nitrate hexahydrate ($Ce(NO_3)_3 \cdot 6H_2O$) dissolved in 250 mL distilled water, where x corresponds to a Ce concentration of 0.1. The suspension was stirred at 500 rpm and 60 °C for 6 h to facilitate uniform dispersion of the cerium precursor. The impregnated material was dried at 100 °C for 12 h and subsequently calcined at 650 °C under N_2 atmosphere in a tube furnace to convert the precursor into active CeO_2. The solid was further dried at 120 °C for 24 h and calcined again at 500 °C for 3 h in air to obtain the final bifunctional Ce/Zeolite catalyst. The physicochemical properties of the catalyst were analyzed using scanning electron microscopy coupled with energy-dispersive X-ray spectroscopy (SEM–EDX), X-ray diffraction (XRD), and Brunauer–Emmett–Teller (BET) surface area analysis to determine morphology, elemental composition, crystallinity, and surface characteristics.

2.4 Esterification-Transesterification Process

Methyl ester was synthesized via simultaneous esterification and transesterification using the bifunctional Ce/Zeolite catalyst. The reaction was conducted in a 250 mL three-neck flask equipped with a condenser and a thermometer to ensure temperature control and prevent methanol evaporation. Prior to the reaction, the catalyst was activated by mixing it with methanol at 40 °C for 40 min under continuous magnetic stirring. Catalyst loading was varied at 3%, 4%, and 5% relative to the total oil weight. A mixture of Palm Acid Oil (PAO) and Waste Cooking Oil (WCO) in a 2:1 volumetric ratio (20 mL PAO and 10 mL WCO) was preheated at 100 °C for 1 h to improve homogeneity and reduce viscosity. The pretreated oil mixture was subsequently reacted with methanol at an oil-to-methanol molar ratio of 1:12 in the presence of the activated catalyst.

The reaction was performed for 3 h at controlled temperatures of 40 °C, 50 °C, and 60 °C under continuous stirring. Upon completion of the reaction, the mixture was transferred to a separating funnel and allowed to settle for 24 h, resulting in the formation of three distinct layers: biodiesel (upper layer), glycerol (middle layer), and catalyst (bottom layer). To enhance phase separation, the mixture was further subjected to centrifugation. The biodiesel layer was collected and heated at 65 °C to remove residual methanol. The final product was analyzed using Gas Chromatography–Mass Spectrometry (GC–MS) to determine the concentration of Fatty Acid Methyl Esters (FAME).

2.5 Analysis of Fatty Acid Methyl Ester

Based on the Gas Chromatography–Mass Spectrometry (GC–MS) analysis, the methyl ester concentration reflects the efficiency of oil conversion into biodiesel. Therefore, accurate determination of the Fatty Acid Methyl Ester (FAME) concentration is essential, as it serves as a key parameter for evaluating biodiesel purity and conversion performance. The methyl ester composition was analyzed using GC–MS. The FAME concentration was calculated using the formula presented below.

$$\text{FFA Conversion (\%)} = \frac{\text{\%FFA before reaction - \%FFA after reaction}}{\text{\%FFA before reaction}} \times 100\% \quad (1)$$

$$\text{Triglycerides conversion(\%)} = \left[\frac{\text{\% GC FAME} \times \text{FAME weight (g)}}{\text{PAO-WCO weight (g)}}\right] \times 100\% \quad (2)$$

$$\text{FAME Concentration (\%)} = \frac{\sum \text{FAME area}}{\sum Area\ (\text{FAME} + \text{non} - \text{FAME})} \times 100\% \quad (3)$$

2.6 Analysis of Free Fatty Acid (%FFA)

A mixture of PAO and WCO at a 2:1 ratio was sampled (10 mL) and transferred into a 100 mL Erlenmeyer flask containing 50 mL of 96% ethanol. Subsequently, three drops of phenolphthalein indicator were added to the mixture. The solution was titrated with 0.6 N NaOH until a persistent pink color was observed, indicating the endpoint of the titration. The Free Fatty Acid (FFA) content was calculated using Eq. (4).

$$\%FFA = \frac{V_{titrant} \times N_{NaOH} \times MW_{FFA}}{1000 \times V_{sample} \times \rho_{sample}} \times 100\% \quad (4)$$

$$\text{MW methyl ester} = [(100\% - \%FFA) \times MW_{FFA} + (\%FFA \times MW_{FFA})] \quad (5)$$

Where $V_{titrant}$ is volume of titrant NaOH(mL), N_{NaOH} normality of NaOH (mol/L), MW_{FFA} molecular weight of the dominant free fatty acid, V_{sample} volume of sample methyl ester (mL), ρ_{sample} density of sample methyl ester (g/mL)

2.7 Analysis of Methyl Ester Viscosity

The kinematic viscosity of the methyl ester was determined using an Ostwald viscometer, with distilled water (aquadest) as the reference fluid. Initially, the flow time of distilled water was measured as it passed between the upper and lower calibration marks of the viscometer. The same procedure was subsequently performed for the methyl ester sample under identical conditions. The viscosity of the methyl ester was calculated using Eq. (6) based on the recorded flow times.

$$\eta = \frac{\rho_x \times t_x}{\rho_a \times t_a} \times \eta_a \quad (6)$$

where η_x is viscosity of methyl ester, η_a viscosity of water, ρ_x density of methyl ester, ρ_a density of water, t_x flow time of methyl ester, t_a flow time of water

2.8 Analysis of Methyl Ester Density

The density of the methyl ester was measured using a pycnometer. The empty pycnometer was first weighed, and its

mass was recorded. It was then completely filled with methyl ester, sealed, and weighed again to obtain the mass of the filled pycnometer. The density of the methyl ester was calculated using Eq. (7) based on the mass difference between the empty and filled pycnometer.

$$\rho = \frac{m_{\text{pycnometer+methyl ester}} - m_{\text{empty pycnometer}}}{V_{\text{pycnometer}}} \quad (7)$$

2.9 Design and Analysis of Experiments Based on Response Surface Methodology

Response Surface Methodology (RSM) is a statistical and mathematical technique employed to evaluate the interactions among multiple independent variables and their effects on one or more response variables. In this study, experimental conditions were designed and optimized using a Central Composite Design (CCD) implemented in Design-Expert software. After establishing the experimental matrix through the RSM–CCD framework, the obtained data were subjected to linear regression analysis to develop an empirical statistical model (Ali *et al*., 2023). Originally introduced by Box and Wilson (1951), RSM integrates statistical and mathematical approaches to systematically design experiments, construct predictive models, assess the significance of factor effects, and determine optimal operating conditions (Almeida *et al*., 2008). This methodology has been extensively applied in biotechnology, industrial processes, and various scientific investigations. In practical applications, RSM involves conducting sequential experimental runs, fitting polynomial models to experimental data, and generating two- and three-dimensional response surface plots to visualize the interaction effects between variables (Malenga *et al*., 2022; Sharma *et al*., 2020).

Central Composite Design (CCD) is a widely adopted fractional factorial design within the RSM framework. It incorporates factorial points, axial ("star") points, and center points to estimate curvature effects and to identify optimal operating conditions for the selected variables. In reaction optimization studies, critical parameters are treated as independent variables and denoted as X_1–X_k (Momen *et al*., 2016). CCD facilitates efficient estimation of both first-order (linear) and second-order (quadratic) effects, providing high predictive accuracy while minimizing the number of experimental runs required (Bhattacharya, 2016). The CCD structure consists of factorial runs (2^k), axial runs (2k), and center points (n_c), where *k* represents the number of investigated factors. All experimental runs were conducted in a randomized order to reduce systematic bias and experimental error. The relationship between the dependent response and the independent variables was described using a second-order polynomial regression model, as expressed in Eq. (8).

$$Y = \beta_0 + \beta_1 X_1 + \ldots + \beta_k X_k + \beta_{12} X_1 X_2 + \beta_{13} X_1 X_3 + \ldots + \beta_{k-1} k X_{k-1} X_k + \beta_{11} X_1^2 + \ldots + \beta_{kk} X_k^2 + \epsilon \quad (8)$$

In this model, *Y* represents the predicted response, whereas X_1 to X_k denote the independent variables. The interaction terms (X_1X_2, X_1X_3, …, $X_{k-1}X_k$) describe the combined effects between variables, while the quadratic terms (X_1^2, …, X_k^2) account for nonlinear influences. The coefficient β_0 corresponds to the intercept or overall mean response, β_1–β_k are the linear regression coefficients of each factor, and ε represents the experimental error associated with the model. The experimental matrix constructed based on this design is presented in Table 1.

3. Result and Discussion

3.1 Catalyst Characterization

3.1.1 X-Ray Diffraction (XRD) Analysis

X-ray diffraction (XRD) provides structural information that distinguishes crystalline and amorphous phases in solid materials. The technique characterizes crystal structures by measuring the diffraction of X-rays interacting with atomic planes within a solid lattice. The resulting diffractogram plots diffraction angle (2θ) versus intensity, producing characteristic peaks corresponding to specific crystalline phases. Diffraction occurs when the X-ray wavelength satisfies Bragg's law relative to the interplanar spacing of the crystal lattice (Ao *et al*., 2024). In this study, XRD was employed to characterize zeolite synthesized from geothermal waste and subsequently impregnated with cerium.

Figure 2. presents the XRD patterns of zeolite and Ce/zeolite (1:10 ratio), processed using Origin software. The parent zeolite exhibited dominant diffraction peaks at 2θ values of 23.07°, 23.77°, 26.39°, 29.85°, 45.39°, and 54.99°, whereas the Ce/zeolite catalyst showed peaks at 23.03°, 23.71°, 28.25°, 29.85°, 45.21°, and 47.35°. These reflections correspond primarily to silica (Si), indicating that the crystalline framework of the geothermal-derived zeolite remained structurally stable following cerium impregnation. In the bifunctional Ce/zeolite catalytic system, the acidic sites of the zeolite promote esterification of free fatty acids (FFA), while cerium species act as basic sites facilitating transesterification of triglycerides into methyl esters (Mulyatun *et al*., 2022). The proposed

Table 1
RSM experimental matrix with two-factor CCD

No		Faktor A	Faktor B
1.		-1	-1
2.	Factorial runs	+1	-1
3.	$2^2 = 4$	-1	+1
4.		+1	+1
5.		+1.41421	0
6.	Axial or star point runs	-1.41421	0
7.	2(2) = 4	0	+1.41421
8.		0	-1.41421
9.	Centre point	0	0
10.		0	0

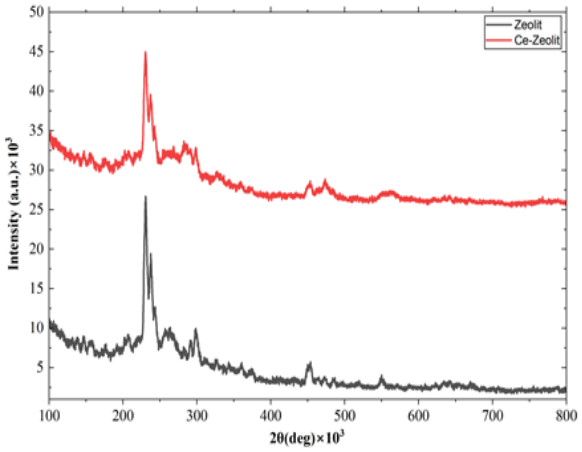

Fig 2. XRD Analysis of Zeolite vs Ce/Zeolite

simultaneous esterification–transesterification mechanism is illustrated in Figure 3.

The dominance of silica-related reflections suggests that the zeolite framework—composed of interconnected SiO_4 and AlO_4 tetrahedra—maintains its crystalline integrity, with a Si:O ratio of 1:2. A higher silica content generally enhances crystallinity and structural stability (Muhammad *et al.*, 2024). Cerium oxide (CeO_2) typically crystallizes in a fluorite-type cubic structure (space group $Fm\bar{3}m$) with a lattice parameter of 5.411 Å at room temperature. However, lattice defects, high dispersion, oxygen vacancies, or incorporation into the zeolite matrix may render cerium species highly dispersed or partially amorphous, thereby reducing their detectability by XRD (Othman *et al.*, 2024). Furthermore, the relatively low Ce loading ratio (1:10) limits the overall intensity of cerium-related reflections. Therefore, complementary analyses such as SEM–EDX are required to verify cerium presence and spatial distribution.

The catalytic performance of acid–base bifunctional systems is strongly governed by the balance between acidic and basic sites. Catalysts with low acid and high base loadings (25:75) demonstrate efficient triglyceride transesterification (Naseef & Tulaimat, 2025); however, when applied to high-FFA and highly saturated feedstocks such as PAO, excessive basicity promotes saponification side reactions. PAO is characterized by high FFA content and a tendency to solidify at ambient temperature, which further complicates phase behavior. Saponification occurs when basic sites react with FFAs and triglycerides to produce soap and glycerol, adversely affecting methyl ester purity and separation efficiency (Azmi *et al.*, 2025). Conversely, catalysts with high acid and low base ratios (75:25) effectively catalyze FFA esterification, but slower triglyceride conversion limits overall FAME formation (Dai *et al.*, 2021). An intermediate acid–base balance (50:50 overall) has been reported to provide optimal synergy, yielding 94–96% FAME across various feedstocks (Yu *et al.*, 2023). However, for dense and high-FFA oils such as PAO, increasing the proportion of basic sites may intensify saponification, leading to gel or semi-solid formation and negatively affecting product viscosity (Azmi *et al.*, 2025). Therefore, a limited base-site ratio (1:10) was selected as the optimal configuration for high-FFA PAO. The relatively low cerium loading provides sufficient basic functionality to facilitate transesterification while minimizing undesirable side reactions. This rationale is supported by the observed relatively high methyl ester viscosity (>5.6–6 cSt, as implied in Table 9), even under a limited base-site ratio (1:10). The elevated viscosity suggests that further increases in base-site density could exacerbate side reactions and compromise product quality. Under the selected condition, effective synergy between esterification and transesterification was achieved, saponification was controlled, and high-quality methyl ester was successfully produced from high-FFA PAO that solidifies at ambient temperature.

3.1.2 Brunaeur-Emmett-Teller (BET) Analysis

The BET method measures the specific surface area of porous solids and powders. This property is critical for materials such as zeolites, where surface texture and porosity influence adsorption and catalytic performance. Developed by Brunauer, Emmett, and Teller, the method is based on multilayer gas adsorption on solid surfaces (Irwansyah *et al.*, 2024). Gas molecules first form a monolayer through physical attraction, and as pressure increases, additional layers form, leading to multilayer adsorption. BET analysis remains a key technique for characterizing porous materials, providing insights into their textural and surface properties that directly affect catalytic activity

Table 2. presents the surface properties of the unmodified zeolite and Ce/zeolite catalysts obtained from BET analysis. Following cerium impregnation, the specific surface area decreased from 146.85 m²/g to 120.61 m²/g, and the total pore volume declined from 0.1409 cc/g to 0.1352 cc/g. Meanwhile, the average pore diameter increased from 3.84 nm to 4.49 nm. Similar trends have been reported by Ginting *et al.* (2023), who

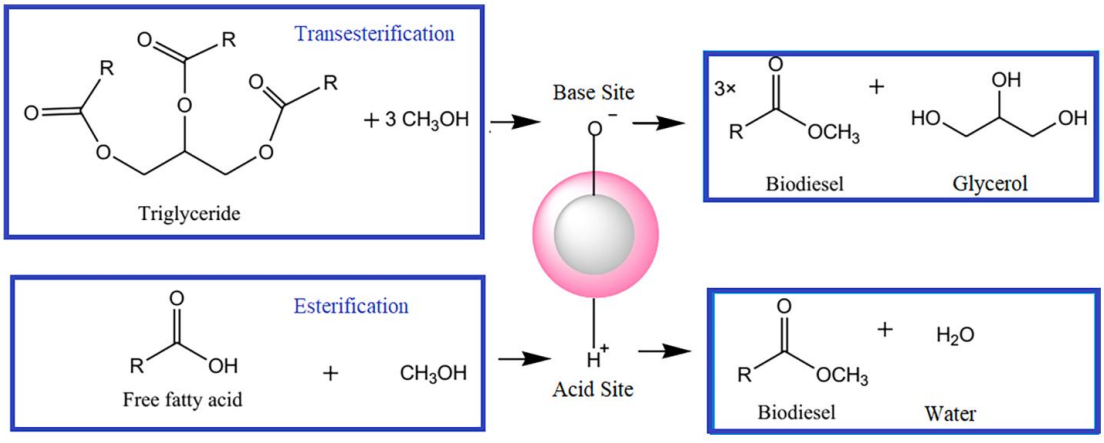

Figure 3. Simultaneous esterification-transesterification reaction with a bifunctional catalyst (Mulyatun *et al.*, 2022)

Table 2.
Surface properties of Zeolite BET catalyst and Ce/Zeolite

Parameter	Zeolite (before impregnation)	Ce/Zeolite (after impregnation)
BET Surface Area	146.85 m^2/g	120.61 m^2/g
Total Pore Volume	0.1409 cc/g	0.1352 cc/g
Average Pore Diameter	3.84 nm	4.49 nm
Micropore Surface Area (t-method)	115.3 m^2/g	90.08 m^2/g
External Surface Area(t-method)	31.54 m^2/g	30.52 m^2/g

observed a reduction in surface area from 46.6406 m^2/g to 34.7985–44.5367 m^2/g after $FeCl_3 \cdot 6H_2O$ modification, depending on the added volume (25–100 mL). This reduction resulted from the formation of new pores that reduced the effective active pore radius. Zeolite treated with 25 mL $FeCl_3 \cdot 6H_2O$ (Ze-25-$FeCl_3$) exhibited the lowest specific surface area (34.7985 m^2/g) and pore volume (0.00606 cc/g), which was attributed to 120 minutes of ultrasonic treatment that enhanced the diffusion and penetration of $FeCl_3 \cdot 6H_2O$ into the zeolite framework. Such treatment may have induced pore widening or localized structural rearrangement, leading to an increase in pore diameter. The decrease in pore volume was associated with metal coverage on the zeolite surface; as a greater amount of metal species occupied the pores, the available internal pore space decreased accordingly. Consequently, surface area and pore volume exhibited an inverse correlation with pore radius (Jian *et al*., 2018).

The reduction in surface area and pore volume of Ce/Zeolite indicates partial pore blockage following cerium incorporation, particularly within the microporous region, as evidenced by the decreased micropore surface area. Meanwhile, the increase in average pore diameter from 3.84 to 4.49 nm may enhance the diffusion of bulky molecules such as triglycerides, thereby improving access to active sites. The relatively unchanged external surface area suggests that cerium species preferentially occupied internal micropores rather than depositing on the outer surface. This behavior is likely driven by strong interactions between cerium precursors and hydroxyl (–OH) groups associated with acid sites along the micropore walls (Borges *et al*., 2013). Similarly, Garcia *et al*. (2011) reported that in Ce-USY systems with low to moderate cerium loading, cerium species predominantly reside at ion-exchange positions within the zeolite framework rather than on the external surface. Cerium was found to reside at cationic sites inherently available within the micropores, further confirming its stabilization inside the internal zeolitic structure.

3.1.3 Scanning Electron Microscope-Energy Dispersive X-Ray (SEM-EDX) Analysis

SEM–EDX analysis was performed to evaluate the elemental composition, surface morphology, and microstructural characteristics of the Ce/Zeolite catalyst. The catalyst, prepared at a Ce:Zeolite ratio of 1:10, was characterized after impregnation and calcination at 650 °C for 3 h to assess its porosity and the dispersion of cerium species on the zeolite surface. The zeolite, synthesized from geothermal waste, was modified through cerium incorporation, and the resulting elemental composition is summarized in Table 3.

Table 3.
EDX Analysis Results of Ce/Zeolite Catalysts

Compound	Mass%
Na	8.57
Al	14.27
Si	76.36
Se	0.52
Ce	0.27

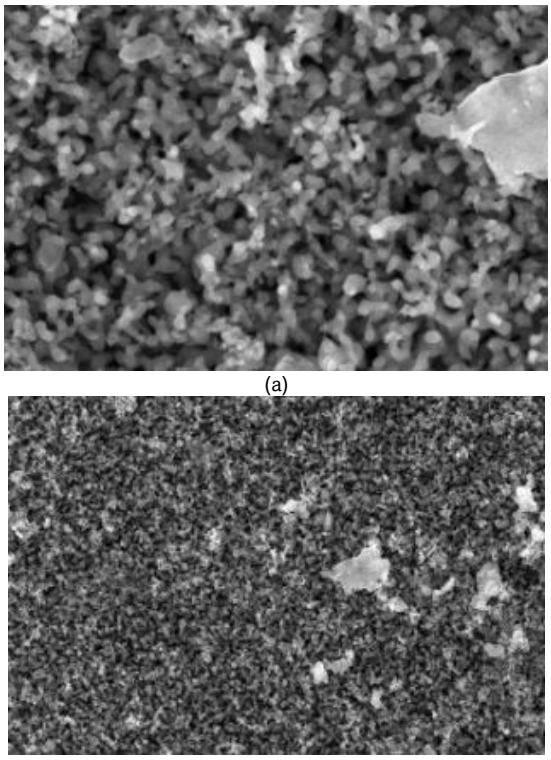

(a)

(b)

Fig 4. SEM-EDX analysis results of Ce/Zeolite catalyst at ×10,000 magnification (a) and ×3,000 magnification (b)

The Ce/Zeolite catalyst contained Si and Al as acid sites and Ce as basic sites. The Si/Al ratio, a critical parameter reflecting zeolite quality, strongly influences crystallinity and catalytic performance (Munfarida *et al*., 2020; Yusof *et al*., 2010). EDX analysis revealed a Si/Al ratio of approximately 5.1, consistent with the aluminosilicate structure of Beta zeolite (Li *et al*., 2023). This ratio indicates the presence of substantial Brønsted acid sites generated by the substitution of Al^{3+} for Si^{4+} in the framework, thereby enhancing esterification activity in high-FFA oils. The detection of cerium confirms successful impregnation, with a Ce/(Si+Al) molar ratio of approximately 0.0006 mol/mol, suggesting that cerium acted as a low-level dopant supplying basic sites for simultaneous esterification–transesterification reactions (Li *et al*., 2025). The experimentally determined Ce content was lower than the theoretical 1:10 loading (≈0.27 wt%), indicating limited impregnation efficiency or partial precursor loss, potentially due to non-uniform CeO_2 dispersion and relatively weak interaction between cerium species and the zeolite framework. The corresponding SEM micrograph is presented in Figure 4.

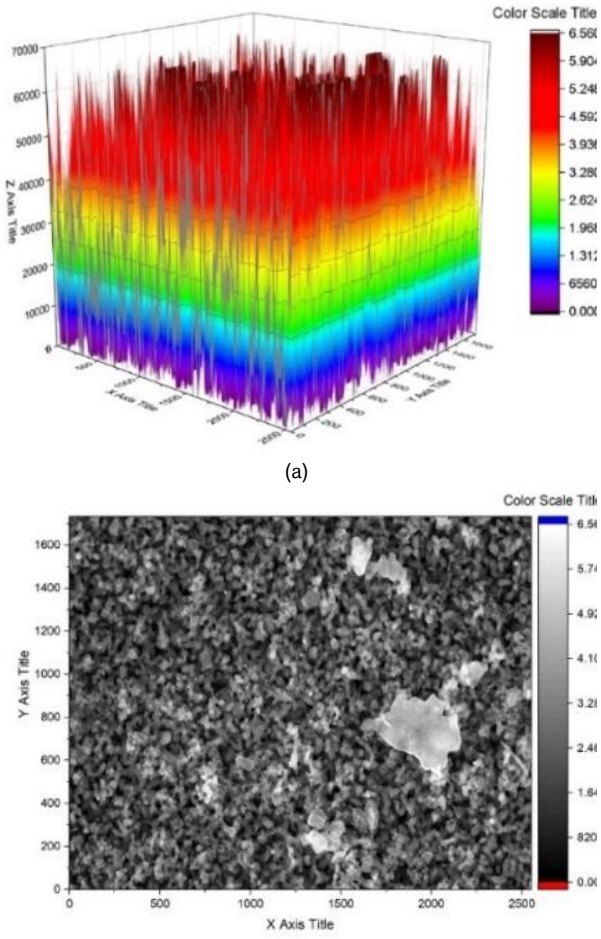

Fig 5. Porosity Analysis of Ce/Zeolite Catalyst

Figure 4. shows the SEM image of the Ce/Zeolite catalyst after impregnation and calcination. The surface exhibits rough, irregular flake-like structures with smaller particles attached to larger agglomerates. The presence of irregular spherical particles suggests dispersed cerium species distributed over the zeolite surface. Particle aggregation likely occurred due to partial CeO_2 sintering during high-temperature calcination, further confirming successful cerium incorporation (Zhang *et al*., 2020). Catalytic performance is strongly influenced by textural characteristics, particularly surface area and pore structure. The formation of inter-aggregate voids observed after calcination, as shown in Figure 4, indicates the development of additional accessible surface regions, which may enhance structural stability and catalytic activity (Schlögl, 2015).

Figure 5. presents the porosity analysis of the Ce/Zeolite catalyst processed using Origin2025. The three-dimensional plot (Figure 5a) illustrates pore distribution, where the x–y axes represent spatial coordinates of the sample and the z-axis corresponds to pore density; red regions indicate higher pore density, while blue regions denote lower density. Figure 5b displays high-resolution surface morphology characterized by irregular spherical pores. The color scale reflects variations in pore depth and density, with darker tones corresponding to denser regions. Overall, Figure 5. evaluates the pore structure and distribution, which play a crucial role in determining mechanical strength, chemical reactivity, and environmental interactions (Erdiwansyah *et al*., 2024). The catalyst exhibited a porosity of 63.78%, classified within the mesoporous range (2–50 nm). This mesoporous structure facilitates diffusion of triglycerides and free fatty acids (FFAs) toward active sites, reduces mass transfer limitations, and enhances overall conversion efficiency. Mesoporous catalysts are generally reported to exhibit approximately twice the esterification activity of microporous catalysts due to improved accessibility of acid–base active sites (Fatimah *et al*., 2023).

3.2 Characteristics of PAO-WCO Raw Materials

This study used a mixture of palm acid oil and waste cooking oil. PAO-WCO with a 2:1 ratio was used as the raw material in the biodiesel production process. The results of the acid-base titration analysis showed that the oil contained 53.214% free fatty acid (FFA). To determine its chemical composition, GC-MS analysis was performed, and the results are presented in Table 4.

Palm Acid Oil (PAO) is a by-product of palm oil refining (Amalina *et al*., 2021). Its fatty acid profile is comparable to that of Palm Fatty Acid Distillate (PFAD) and varies depending on feedstock type and refining conditions. PAO contains both saturated and unsaturated fatty acids. Saturated fatty acids—including lauric, myristic, palmitic, and stearic acids—are typically solid at room temperature, whereas unsaturated fatty acids such as palmitoleic, oleic, linoleic, and linolenic acids remain liquid (Buchori *et al*., 2022). As shown in Table 1., the PAO used in this study predominantly consists of palmitic, oleic, linolenic, and stearic acids. The high free fatty acid (FFA) content of PAO enhances its suitability for conversion into fatty acid methyl esters (FAME), demonstrating strong potential as a biodiesel feedstock (Buchori *et al*., 2022). However, the elevated FFA level also presents challenges during transesterification due to the increased risk of saponification.

Waste Cooking Oil (WCO) differs chemically from fresh oil due to thermal oxidation, hydrolysis, and polymerization reactions occurring during frying. Nevertheless, WCO generally meets biodiesel feedstock standards in terms of density, acid value, viscosity, and iodine number (Monika *et al*., 2023). As

Table 4.
Fatty acid composition of PAO raw material

Fatty acid	Molecular weight	Composition (%)
Decanoic acid ($C_{10}H_{20}O_2$)	172	-
Palmitoleic acid ($C_{16}H_{30}O_2$)	254	0.2
Myristic acid ($C_{14}H_{28}O_2$)	228	1.38
Stearic acid ($C_{18}H_{36}O_2$)	284	4.64
Lauric acid ($C_{12}H_{24}O_2$)	200	0.23
Palmitic acid ($C_{16}H_{32}O_2$)	256	52.25
Linolenic acid ($C_{18}H_{30}O_2$)	280	9.63
Oleic acid ($C_{18}H_{34}O_2$)	282	31.26
Linoleic acid ($C_{18}H_{32}O_2$)	278	0.41
Arachidonic acid	312	-
Arachidonic acid	368	-

Table 5
Dominant fatty acid composition of WCO raw material

Fatty acid	Molecular weight	Composition (%)
Palmitic acid ($C_{16}H_{32}O_2$)	256	34.74
Oleic acid ($C_{18}H_{34}O_2$)	282	11.82
Stearic acid ($C_{18}H_{36}O_2$)	284	46.7

shown in Table 5, WCO primarily contains palmitic, oleic, and stearic acids, with palmitic and stearic acids classified as saturated fatty acids and oleic acid as an unsaturated fatty acid. Although WCO typically exhibits elevated FFA content, viscosity, and saponification index, these parameters directly influence biodiesel yield and product quality (Monika *et al*., 2023).

High FFA levels may hinder large-scale methyl ester production by promoting soap formation, which interferes with phase separation and reduces conversion efficiency. WCO also generally presents high kinematic viscosity, saponification index, flash point, moisture content, and FFA level, all of which significantly affect biodiesel yield and quality (Monika *et al*., 2023). In this study, the PAO–WCO mixture (2:1 v/v) exhibited a high FFA content of 53.21%, confirming the necessity of an effective catalytic system capable of simultaneously promoting esterification and transesterification while minimizing saponification. Therefore, reducing FFA levels is essential to prevent soap formation and improve conversion efficiency.

Temperature plays a critical role in FFA conversion. Elevated temperatures enhance mass transfer and increase reactant solubility, thereby accelerating reaction kinetics through increased molecular mobility. However, FFA conversion is not governed solely by temperature. It is also influenced by mass transfer limitations between catalyst and reactants, as well as methanol vaporization at higher temperatures, which can reduce effective reactant concentration and overall reaction efficiency (Maafa *et al*., 2022).

3.3 Experimental Design and Statistical Analysis of FAME Contents Using Response Surface Methodology

Analysis of Variance (ANOVA) was employed to assess the statistical significance of individual factors and their interaction effects on FAME yield, thereby identifying the variables that most strongly influenced the methyl ester synthesis process (Bouyakhsass *et al*., 2023). Reaction temperature (A) and catalyst loading (B, wt%) were selected as the principal operating parameters. The empirical second-order polynomial model generated using Design Expert 13.0 is expressed in Eq. (9).

$$\text{FAME Yield (Y)} = 90.66 + 1.62A - 0.96B - 1.19AB - 2.3A^2 - 2.03B^2 \quad (9)$$

In the regression equation, positive coefficients indicate synergistic or enhancing effects, whereas negative coefficients represent antagonistic or inhibitory influences (Mohammadi *et al*., 2023). The magnitude of each coefficient reflects the relative contribution of the corresponding factor to the response (Bouyakhsass *et al*., 2023). Temperature (A) exhibited the highest positive coefficient (+1.62), confirming its dominant influence on reaction kinetics and overall conversion. The quadratic term (A^2) indicates the existence of an optimum temperature range within the experimental domain. In contrast, catalyst loading (B) showed a smaller negative linear effect (−0.96), while its quadratic term (−2.03) suggests a decline in efficiency beyond the optimum loading, likely due to active site saturation and mass transfer limitations. Model adequacy was evaluated using R^2, adjusted R^2, predicted R^2, and Adeq Precision values.

Table 6.
Response Surface Methodology experimental matrix on FAME content analysis

Run	No coding		With coding		%FAME
	X_1	X_2	X_1	X_2	
1	50	4	0	0	91.34
2	40	5	-1	+1	85.4
3	60	5	+1	+1	85.15
4	50	5.4142	0	+1.4142	90.57
5	60	3	+1	-1	88.55
6	64.142	4	+1.4142	0	89.68
7	50	4	0	0	89.98
8	40	3	-1	-1	84.03
9	35.858	4	-1.4142	0	83.54
10	50	2.5858	0	-1.4142	83.72

Table 6. presents the experimental design matrix generated using Design Expert 13.0 for the development of the second-order polynomial model (Bouyakhsass *et al*., 2023). The Central Composite Design consisted of ten experimental runs: four factorial points, four axial points, and two center points.

Table 7. presents the model comparison based on Sequential Sum of Squares analysis. The sequential p-values for the linear, two-factor interaction (2FI), quadratic, and cubic models were 0.2532, 0.4537, 0.1856, and 0.1450, respectively. Although the quadratic and cubic models exhibited lower p-values, the quadratic model was selected as the most appropriate representation due to its balanced statistical performance, nonsignificant Lack of Fit, reasonable model complexity, and absence of aliasing. Accordingly, Design Expert recommended the quadratic model as the most suitable representation of the FAME response.

The statistical evaluation yielded $R^2 = 0.7371$, Adjusted $R^2 = 0.4086$, Predicted $R^2 = -0.8362$, and Adeq Precision = 4.3679. An R^2 value of 0.7371 indicates that 73.71% of the variation in FAME content is explained by the experimental variables and their interactions, while 26.29% is attributed to uncontrolled or external factors (Ghelich *et al*., 2019). A regression coefficient exceeding 70% suggests that the model remains applicable for analytical purposes. The Adeq Precision value of 4.3679 (>4) confirms an adequate signal-to-noise ratio and acceptable model discrimination capability. Although the Predicted R^2 is negative (−0.8362), the model can still be utilized to identify local optimum conditions within the investigated design space, particularly for evaluating parameter trends and response tendencies. The moderate R^2 value indicates acceptable agreement between experimental and predicted data within the

Table 7.
Sequential model of SUM in FAME Yield analysis

Source	Sequential p-value	Lack of Fit p-value	Adjusted R^2	Predicted R^2	
Linear	0.2532	0.2325	0.1316	-0.2749	
2FI	0.4537	0.2219	0.0847	-0.9128	
Quadratic	0.1856	0.2540	0.4086	-0.8362	Suggested
Cubic	0.1450	0.3538	0.8285	-0.8026	Aliased

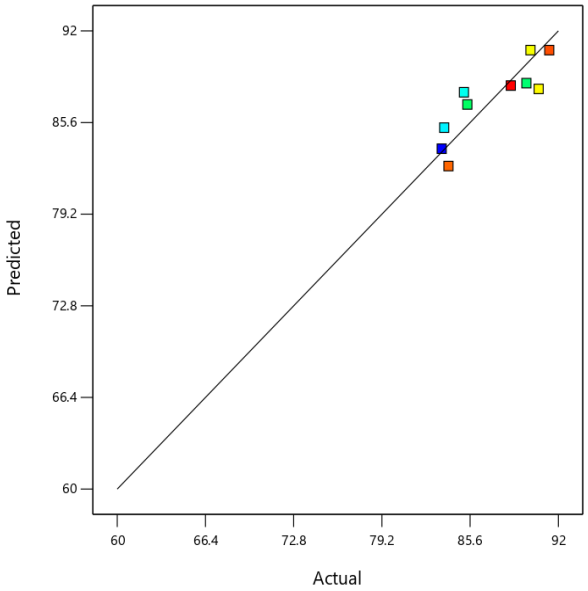

Fig 6. Predicted vs actual FAME yield data

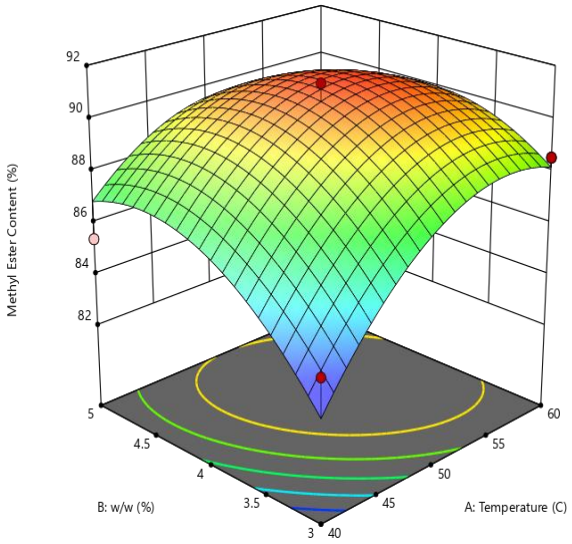

Fig 7. Response surface plots for FAME concentration

studied domain. Therefore, the model is suitable for determining optimum conditions within the defined experimental range (Yudiastuti *et al*., 2024). In this study, the model is applied in a qualitative–semi-quantitative manner to interpret system behavior, focusing on directional effects (increasing or decreasing trends), factor interactions, general response tendencies, and localization of the optimum region (Uche *et al*., 2024). Within this context, the model provides meaningful mechanistic insight despite its limited external predictive capability.

Figure 6. illustrates the model adequacy evaluated through ANOVA. A statistically valid model is characterized by significant ANOVA results and acceptable determination coefficients. The p-value determines the contribution of each factor to methyl ester yield, while model adequacy is assessed using the coefficient of determination (R^2) (Akhabue *et al*., 2022). The R^2 value of 0.7371 confirms that 73.71% of the variability in FAME content is explained by the model, whereas 26.29% remains influenced by external factors. The correlation between predicted and actual FAME values is also presented in Figure 6., demonstrating satisfactory agreement, with deviations primarily attributed to random experimental variability.

3.4 Effect of the Significant Interacting Variables on the FAME Concentrations

The influence of statistically significant interacting variables on FAME yield was analyzed using the response surface plots shown in Figure 7. The three-dimensional surface illustrates the interaction between reaction temperature and catalyst loading. The RSM model depicted in Figure 7. consistently reflects the experimental trends reported in Table 8. The region of elevated FAME content corresponds to conditions under which effective FFA reduction and triglyceride (TG) conversion occur simultaneously, in agreement with the bifunctional catalytic mechanism. Thus, Table 8. experimentally validates the optimum region predicted by the response surface analysis.

FAME content (%) increased progressively as catalyst loading increased from 3% wt to 4% wt, followed by a decline when catalyst loading exceeded 4% wt. The enhancement observed within the 3–4% range can be attributed to the increased number of available active sites, which accelerated reaction kinetics and shifted the equilibrium toward methyl ester formation (Fadhil *et al*., 2016). The high catalytic activity is associated with hydrophilic functional groups (–COOH, –OH, –SO_3H) present on the catalyst surface, which serve as active centers for esterification and transesterification reactions. A higher density of active sites increases the probability of effective molecular collisions, thereby facilitating faster attainment of equilibrium (Kusumaningtyas *et al*., 2023). However, at catalyst loadings above 4% wt, FAME yield decreased due to increased mixture viscosity and diminished mass transfer efficiency resulting from excessive solid catalyst presence. In heterogeneous catalytic systems, the overall reaction rate is strongly influenced by both intrinsic surface reactions and external mass transfer phenomena. Excess catalyst can increase diffusion resistance and reduce effective reactant accessibility to active sites, thereby lowering overall efficiency (Okechukwu *et al*., 2022).

Reaction temperature also exerted a significant influence on FAME yield. Increasing the temperature from 40°C to 55°C enhanced molecular kinetic energy and reactant solubility, thereby accelerating reaction rates (Maafa, 2022). Nevertheless, FAME content decreased at temperatures above 55°C due to methanol vaporization, which altered the optimal alcohol-to-oil molar ratio (Farouk *et al*., 2024). Elevated temperatures may additionally hinder liquid–solid mass transfer efficiency, resulting in decreased catalytic performance (Maafa, 2022). Overall, temperature demonstrated a more dominant and relatively linear influence on FAME formation compared to catalyst loading within the investigated range.

3.5 Quantitative Correlation of FFA and TG Conversion with FAME Content

A quantitative evaluation was performed to examine the relationship between FFA reduction, triglyceride (TG) conversion, and the resulting FAME yield. In a single-step esterification–transesterification system, FAME formation is governed by the simultaneous conversion of both FFA and triglycerides. Therefore, analyzing the interdependence among these parameters provides a comprehensive assessment of the overall catalytic performance.

Table 8.
FAME concentration, FFA conversion and TG conversion values

	%FFA conversion	%TG conversion	%FAME
Run 1 (50℃, 4% wt Ce/Zeolite)	25.14	49.30	91.34
Run 2 (40℃, 5% wt Ce/Zeolite)	31.29	31.58	85.40
Run 3 (60℃, 5% wt Ce/Zeolite)	25.18	26.87	85.15
Run 4 (50℃, 5,4% wt Ce/Zeolite)	24.33	43.46	90.57
Run 5 (60℃, 3% wt Ce/Zeolite)	30.43	51.87	88.55
Run 6 (64℃, 4% wt Ce/Zeolite)	28.42	31.09	89.68
Run 7 (50℃, 4% wt Ce/Zeolite)	24.27	43.11	89.98
Run 8 (40℃, 3% wt Ce/Zeolite)	27.95	48.49	84.03
Run 9 (36℃, 4% wt Ce/Zeolite)	20.14	17.81	83.54
Run 10 (50℃, 2,5% wt Ce/Zeolite)	30.38	25.92	83.72

Mechanistically, Figure 3 illustrates that the bifunctional Ce/Zeolite catalyst operates via two concurrent pathways: (i) esterification of FFA over acidic sites and (ii) transesterification of triglycerides over basic sites. This dual-function mechanism provides the mechanistic framework for interpreting the quantitative data presented in Table 8. The consistently measurable FFA conversion across all experimental runs confirms the activity of the acid sites, whereas the observed TG conversion (reaching 51.87% in Run 5) demonstrates that the basic sites are also catalytically active. Collectively, these results verify that the catalyst exhibits genuine bifunctional behavior, as illustrated in Figure 3.

FFA conversion increased as the temperature rose from 35 °C to 60 °C due to enhanced molecular kinetic energy, which accelerated reaction rates (Maafa, 2022). The highest FFA conversion of 31.30% was obtained at 40 °C (Run 2). Above 50 °C, conversion declined, primarily because methanol vaporization near its boiling point reduced effective liquid-phase reactivity (Kusumaningtyas *et al*., 2023). These observations indicate that conversion is not solely governed by temperature; mass-transfer limitations and methanol evaporation also influence the reaction system (Maafa, 2022). Increasing catalyst loading from 3 wt% to 5 wt% improved FFA conversion by increasing the number of accessible active sites and shifting the equilibrium toward product formation (Fadhil *et al*., 2016; Kusumaningtyas *et al*., 2023). However, excessive acidity in the Ce/Zeolite catalyst (Ce:Zeolite = 1:10) promoted reverse esterification and saponification reactions, thereby lowering catalytic efficiency (Shobhana-Gnanaserkhar *et al*., 2020). Furthermore, excess methanol reduced conversion by diluting reactants and facilitating the formation of inactive sulfonate esters (Zhang *et al*., 2021).

Triglyceride conversion also increased with temperature from 35 °C to 60 °C, reaching a maximum of 51.87% at 60 °C (Run 5). Elevated temperatures enhanced molecular collisions and intrinsic reaction rates; however, TG conversion decreased to 31.09% at 64 °C (Run 6), likely due to intensified saponification and methanol vaporization. The optimal temperature range of 50–60 °C is consistent with previous findings (Lira & Atadashi, 2018; Maafa, 2022). TG conversion was likewise influenced by catalyst loading, with the highest value (51.87%) observed at 3 wt%. Increasing catalyst dosage enhanced adsorption capacity and surface reaction rates (Widiarti *et al*., 2019). Nevertheless, excessive catalyst promoted ester hydrolysis and saponification, thereby reducing overall yield. Although zeolite exhibits structural stability and tunable acidity suitable for metal oxide modification, excessively high calcination temperatures may decrease surface area and catalytic activity (Mazaheri *et al*., 2021).

The quantitative relationship among FAME concentration, FFA conversion, and TG conversion (Table 8) demonstrates that FAME content increases with higher TG and FFA conversions, although TG conversion exerts the more pronounced effect. The highest FAME concentration (91.34%) was achieved at 49.30% TG conversion and 25.14% FFA conversion, whereas the lowest FAME concentration (83.72%) corresponded to 25.92% TG conversion and 30.38% FFA conversion. These results indicate that FAME formation is predominantly driven by triglyceride transesterification (Farooq *et al*., 2015). From a chemical standpoint, FAME is generated through the simultaneous esterification of FFA and transesterification of triglycerides catalyzed by the bifunctional Ce/Zeolite system, in which acidic sites promote FFA conversion and basic sites facilitate TG conversion (Leung *et al*., 2010). Empirical data further reveal a stronger positive correlation between FAME concentration and TG conversion than with FFA conversion; increasing TG conversion from approximately 25% to 50% elevated FAME content from about 84% to above 90%, underscoring the dominant contribution of TG conversion (Domínguez-Barroso *et al*., 2024). These findings align with previous studies demonstrating that TG conversion is the principal determinant of total FAME yield, while FFA conversion provides a secondary contribution.

Triglyceride conversion is not the sole pathway for FAME formation from PAO–WCO feedstock, as FAME is simultaneously produced through FFA esterification over acid sites. The observed TG conversion confirms that the Ce/Zeolite catalyst retains basic functionality alongside its acidic character, thereby validating its bifunctional nature within a single-step reaction system. In feedstocks with very high FFA content (53.21%), esterification generally dominates the initial reaction stage and can influence subsequent transesterification. Nevertheless, the measurable TG conversion observed in this study confirms that the catalyst's base sites remain active and contribute meaningfully to FAME production. Compared with previous studies employing feedstocks containing 10–25% FFA, which typically require multiple esterification steps to satisfy SNI 7182 biodiesel standards, the present work utilized a more challenging feedstock (53.21% FFA) and achieved substantial FFA reduction in a single esterification step (from 53.21% to 39.74%). Although TG conversion has not yet become the sole dominant pathway, the bifunctional Ce/Zeolite catalyst demonstrates strong effectiveness in reducing FFA in high-acid feedstocks and offers potential to simplify conventional multi-step esterification processes.

3.6 Optimization of Reaction Conditions Based on Temperature and Catalyst Loading

Numerical optimization was conducted to identify the operating conditions that maximize FAME concentration. The optimal conditions predicted by the model corresponded to a methanol-to-oil molar ratio of 12:1, catalyst loading of 4 wt.%, reaction temperature of 50 °C, and reaction time of 180 min. Under these conditions, the model predicted a maximum FAME concentration of 91.34%, FFA conversion of 25.14%, and TG conversion of 49.3%. Validation experiments performed in

triplicate under the optimized conditions yielded an average FAME concentration of 91.5%, maximum FFA conversion of 25.31%, and maximum TG conversion of 48.72%, confirming accuracy between experimental results and model predictions.

3.7 Characteristics of Fatty Acid Methyl Ester Products

The physicochemical properties of the produced fatty acid methyl ester (FAME) were evaluated based on four key parameters: FAME concentration (%FAME), free fatty acid content (%FFA), kinematic viscosity, and density. Density and viscosity were measured to assess compliance with the Indonesian National Standard (SNI 7182-2015) for biodiesel quality. In contrast, FFA analysis was conducted to evaluate the effectiveness of the esterification stage, particularly in reducing the initially high free fatty acid content of the PAO–WCO feedstock. The measured density, viscosity, %FFA, and %FAME values are summarized in Table 9. According to SNI 7182-2015, high-quality biodiesel must exhibit a density in the range of 0.85–0.90 g/mL (850–890 kg/m³) and a kinematic viscosity of 2.3–6.0 cSt.

As shown in Table 9, only a limited number of experimental runs approached the specified biodiesel quality criteria. Among all runs, Run 5 and Run 8 produced viscosity and density values within or very close to the acceptable range. Run 5 exhibited a viscosity of 5.60 cSt and a density of 890.95 kg/m³, whereas Run 8 showed a viscosity of 5.65 cSt and a density of 877.77 kg/m³. These values fall within the permissible viscosity range and are reasonably close to the specified density limits, indicating partial compliance with SNI standards.

The initial FFA content of the PAO–WCO mixture was 53.21%, representing a highly acidic feedstock that necessitates an efficient esterification process. After the simultaneous esterification–transesterification reaction, the FFA level decreased significantly, reaching a minimum value of 36%. This reduction confirms that esterification occurred effectively and that a substantial fraction of the initially high FFA content was converted. Nevertheless, the residual FFA content remains considerably higher than the permissible limit for biodiesel applications. SNI 7182-2015 specifies a maximum FFA value of 0.8%, while international standards such as ASTM D7467 and EN 14214 require FFA levels below 0.5% (Roza *et al*., 2025). Therefore, further process optimization is required to achieve FFA levels that comply with established specifications.

In principle, zeolite-based bifunctional catalysts are expected to substantially reduce FFA due to the presence of acidic active sites that promote esterification (Leung *et al*., 2010). The relatively high residual FFA observed in this study may be attributed to insufficient reaction time, a non-optimized methanol-to-oil molar ratio, or diffusion limitations inherent to heterogeneous catalytic systems. Furthermore, the relatively low Ce content at the applied Ce:Zeolite ratio of 1:10 may limit the availability of basic active sites, thereby constraining overall transesterification efficiency and FAME formation. In Run 5, the use of 3 wt.% catalyst enabled the simultaneous esterification–transesterification process and reduced the FFA level to 37%. However, increasing catalyst loading to 4 wt.% in Run 7 did not further reduce FFA, which remained at 40%, and was accompanied by increased viscosity and density. As reported by Xie *et al*. (2019), excessive catalyst loading may induce diffusion limitations between methanol, oil, and solid catalyst particles. Higher catalyst concentrations can increase mixture viscosity, thereby restricting mass transfer of reactants to active sites. In addition, excessive catalyst may promote saponification reactions, in which FFAs react with basic sites to form soap-like by-products that complicate phase separation and reduce biodiesel yield (Widayat *et al*., 2024).

According to SNI 7182-2015, biodiesel must contain a minimum methyl ester content of 96.5% (%FAME). In the present study, the maximum %FAME achieved was 91.5%, which does not satisfy the SNI requirement. Previous investigations have demonstrated that bifunctional catalysts applied to feedstocks with initial FFA contents of 10–25% can effectively reduce FFA to below 1% or close to 0.8%, thereby meeting both SNI and ASTM standards. For example, biodiesel production from off-grade crude palm oil (CPO) using a K_2O/Zeolite-Y catalyst under identical methanol ratios, 4 h reaction time, and 60°C reduced FFA from 13% to 0.7%, achieving a %FAME of 95.05% (Sumari *et al*., 2024). Similarly, biodiesel production from waste cooking oil using a bifunctional nanocatalyst derived from palm kernel shell at 80°C for 4 h reduced FFA from 15% to 0.4%, corresponding to 97.3% FFA conversion (Abdullah *et al*., 2020). In contrast, the feedstock employed in this study contained a substantially higher initial FFA level of 53.21%, which represents a more challenging reaction system. Such a high FFA concentration requires longer reaction times, higher methanol-to-oil molar ratios, and potentially increased Ce loading to provide sufficient basic active sites for effective transesterification. These constraints explain why the final FFA content remained at 36% despite significant reduction from the initial value. The substandard %FAME is attributed to the presence of unconverted glyceride species, including monoglycerides, diglycerides, and triglycerides, which remain in the crude biodiesel and require additional purification steps (Niawanti & Zullaikah, 2018).

Density and viscosity are critical parameters influencing fuel atomization, evaporation, air–fuel mixing, combustion efficiency, and emission characteristics. Elevated viscosity may lead to poor atomization, injector fouling, deposit formation, and soot accumulation in engines. Biodiesel viscosity generally

Table 9
FAME characteristics analysis results

	Test parameters			
	Density (kg/m³)	Viscosity (cSt)	%FFA	%FAME
SNI	850-900	2.3-6		≥ 96.5%
Run (Optimization)	894.38	5.626	39.745	91.5
Run 1 (50°C, 4% wt Ce/Zeolite)	895.52	5.724	39.834	91.34
Run 2 (40°C, 5% wt Ce/Zeolite)	912.08	7.081	36.56	85.4
Run 3 (60°C, 5% wt Ce/Zeolite)	899.87	6.323	39.814	85.15
Run 4 (50°C, 5,4% wt Ce/Zeolitee)	925.75	7.321	40.265	90.57
Run 5 (60°C, 3% wt Ce/Zeolite)	890.96	5.604	37.021	88.55
Run 6 (64°C, 4% wt Ce/Zeolite)	903.89	6.363	38.093	89.68
Run 7 (50°C, 4% wt Ce/Zeolite)	910.91	6.589	40.296	89.98
Run 8 (40°C, 3% wt Ce/Zeolite)	877.77	5.657	38.343	84.03
Run 9 (36°C, 4% wt Ce/Zeolite)	905.09	6.536	42.498	83.54
Run 10 (50°C, 2,5% wt Ce/Zeolite)	911.28	6.695	37.046	83.72

increases with higher degrees of unsaturation, particularly in the presence of multiple double bonds. Increased viscosity affects volumetric flow rate and spray characteristics during injection. At low temperatures, excessive viscosity may also compromise the mechanical performance of the fuel injection system. Biodiesel typically exhibits higher density than conventional diesel, which can influence combustion behavior. Density may further increase in biodiesel containing unsaturated fatty acids with more than two double bonds, potentially resulting in incomplete evaporation and less efficient combustion after injection (Kosuru *et al*., 2024).

4. Conclusion

Zeolite was successfully synthesized from geothermal waste, thereby enhancing resource valorization and supporting sustainable material utilization in line with the Sustainable Development Goals (SDGs). The synthesized zeolite was subsequently modified via cerium impregnation to produce a bifunctional Ce/Zeolite catalyst capable of promoting simultaneous esterification and transesterification within a single reaction system. The one-step esterification–transesterification process yielded a maximum FAME concentration of 91.5%, with triglyceride (TG) conversion reaching 48.72%. The free fatty acid (FFA) content of the feedstock was reduced from 53.21% to 39.74%, corresponding to an FFA conversion of 25.14% and an absolute FFA reduction of 13.47%. This reduction is particularly significant considering the very high initial FFA level (53.21%) of the PAO–WCO feedstock. Compared with previous studies that required multiple esterification stages to achieve comparable reductions, the present work demonstrates that substantial FFA mitigation can be achieved in a single reaction step. This finding confirms the critical contribution of the acidic function of the bifunctional Ce/Zeolite catalyst in processing high-FFA feedstocks. Despite the significant FFA reduction, the final %FAME did not yet meet the SNI minimum requirement, primarily due to the presence of unconverted glyceride species (monoglycerides, diglycerides, and triglycerides) remaining in the crude biodiesel phase. This indicates that further reaction intensification and downstream purification are required. To achieve %FAME levels compliant with SNI standards, longer reaction times, higher methanol-to-oil molar ratios, and increased cerium loading are necessary to provide a greater density of basic active sites, thereby enhancing transesterification efficiency and overall FAME formation. Reaction temperature variation was performed to assess the influence of thermal energy on methyl ester production. Increasing the temperature from 40 °C to 50 °C improved mass transfer and reaction kinetics in the esterification–transesterification system, promoting triglyceride conversion and resulting in the highest methyl ester yield. Catalyst loading also significantly influenced process performance. The optimum catalyst loading was identified at 4 wt%, at which the maximum methyl ester yield was obtained.

Acknowledgments

The authors would like to express their sincere gratitude's to the Diponegoro University, Semarang, Indonesia for the financial support. We also wish to acknowledge the Advanced Material Laboratory - Central Laboratory for Research and Service Diponegoro University (CORESDU) for facilitating all the practical processes of this research.

Author Contributions: A.S.N.S.: Writing – review & editing, Writing–original draft, Resources, Project administration, Methodology, Investigation, Formal analysis, Data curation. D.P.W.: Writing – review & editing, Writing–original draft, Resources, Conceptualization. W.W.: Conceptualization, Validation, Supervision, Writing – review & editing. H.H.: Writing – review & editing, Validation. S.S.: Writing – review & editing, Validation. N.N.: Writing – review & editing, Validation.

Conflicts of Interest: The authors declare no conflict of interest.

References

Abdullah, R. F., Rashid, U., Ibrahim, M. L., Hazmi, B., Alharthi, F. A., & Nehdi, I. A. (2021). Bifunctional nano-catalyst produced from palm kernel shell via hydrothermal-assisted carbonization for biodiesel production from waste cooking oil. *Renewable and Sustainable Energy Reviews*, 137, 110638. https://doi.org/10.1016/j.rser.2020.110638.

Abdullah, R. F., Rashid, U., Taufiq-Yap, Y. H., Ibrahim, M. L., Ngamcharussrivichai, C., & Azam, M. (2020). Synthesis of bifunctional nanocatalyst from waste palm kernel shell and its application for biodiesel production. *RSC Advances*, 10(45), 27183–27193. https://doi.org/10.1039/d0ra04306k

Akhabue, C.E., Ukponahiusi, U.J, Osa-Benedict, E O., Otoikhian, S. K., Inetiaribor, O.C., Oyedoh, E.A. (2022). Simultaneous Esterification and Transesterification of Neem Seed Oil Using Ferric Sulphate Doped with Poultry Droppings as a Bifunctional Catalyst. *Front. Energy Res.,* 10. https://doi.org/10.3389/fenrg.2022.927467.

Akream, N. S., Hamd, M. I., Gheni, S. A., Al-Sudani, F. T., Mohammed, A. E., Mohammed, H. R., Ali, M. M., Ahmed, S. M. R., Türköz Karakullukçu, N., & Tahah, A. K. (2024). High-yield activated carbon based ZnO-Ce bifunctional catalyst for production of biodiesel from waste cooking oil. *Energy Conversion and Management,* 321. https://doi.org/10.1016/j.enconman.2024.119054.

Ali, M., Kumar, A., Yvaz, A., & Salah, B. (2023). Central composite design application in the optimization of the effect of pumice stone on lightweight concrete properties using RSM. *Case Studies in Construction Materials,* 18, e01958. https://doi.org/10.1016/j.cscm.2023.e01958.

Amalina, I. F., Haziq, J. M., Syukor, A. A., Ridwan, A. A., & Rashid, A. M. (2021). Study of Palm Acid Oil (PAO) from Sludge Palm Oil Mill Effluent (POME) as Goat's Feed. *Materials Today Proceedings*, 41, 96–101. https://doi.org/10.1016/j.matpr.2020.11.1013.

Ao, S., Gouda, S. prasad, Selvaraj, M., Boddula, R., Al-Qahtani, N., Mohan, S., & Rokhum, S. L. (2024). Transesterification of Jatropha curcas oil to biodiesel using highly porous sulfonated biochar catalyst: Optimization and characterization dataset. *Data in Brief,* 53, 110096. https://doi.org/10.1016/j.dib.2024.110096.

Azmi, M.N.S., Abed, K.M., Putra, S.S.S., Saleh, J., Alanazi, Y.M., Gupta, B.S., Hamid, M.D., Basirun, W.J., Hayyan, A., & Salleh, M.Z.M. (2025). Soap removal from crude biodiesel using industrial polyols. *Journal of Molecular Liquids*, 442, 126972. https://doi.org/10.1016/j.molliq.2025.126972.

Borges, L. D., Moura, N. N., Costa, A. A., Braga, P. R., Dias, J. A., Dias, S. C., De Macedo, J. L., & Ghesti, G. F. (2013). Investigation of biodiesel production by HUSY and Ce/HUSY zeolites: Influence of structural and acidity parameters. *Applied Catalysis a General,* 450, 114–119. https://doi.org/10.1016/j.apcata.2012.10.009.

Bouyakhsass, R., Souabi, S., Rifi, S. K., Bouaouda, S., Taleb, A., Madinzi, A., Kurniawan, T. A., & Anouzla, A. (2023). Applicability of central composite design and response surface methodology for optimizing treatment of landfill leachate using coagulation-flocculation. *Chemical Engineering Research and Design,* 197, 669-684. https://doi.org/10.1016/j.cherd.2023.08.001.

Buchori, L., Widayat, W., Hadiyanto, H., Satriadi, H., Chasanah, N., & Kurniawan, M. R. (2022). Modification of magnetic nanoparticle lipase catalyst with impregnation of Activated Carbon Oxide (ACO) in biodiesel production from PFAD (Palm Fatty Acid Distillate). *Bioresource Technology Reports,* 19, 101137. https://doi.org/10.1016/j.biteb.2022.101137.

Dai, Y., Li, Y., Jia-Hao-Lin, Chen, B. Y., & Chen, C. (2021). One-pot synthesis of acid-base bifunctional catalysts for biodiesel production. *Journal of Environmental Management*, 299, 113592. https://doi.org/10.1016/j.jenvman.2021.113592.

Domínguez-Barroso, V.; Herrera, C.; Larrubia, M.Á.; Gonzalo López, C.; Ramos, D.B.; Alemany, L.J. (2024). Heterogeneization of biodiesel production by simultaneous esterification and transesterification of oleins. *Catalysts* 2024, 14, 871. https://doi.org/10.3390/catal14120871.

Erdiwansyah., Gani, A., Desvita, H., Mahidin., Viena, V., Mamat, R., & Sardjono, R. E. (2024). Analysis study and experiments SEM-EDS of particles and porosity of empty fruit bunches *Case Studies in Chemical and Environmental Engineering,* 9, 100773. https://doi.org/10.1016/j.cscee.2024.100773.

Fadhil, A. B., Aziz, A. M., & Al-Tamer, M. H. (2016). Biodiesel production from Silybum marianum L. seed oil with high FFA content using sulfonated carbon catalyst for esterification and base catalyst for transesterification. *Energy Conversion and Management,* 108, 255–265. http://dx.doi.org/10.1016/j.enconman.2015.11.013.

Farooq, M., Ramli, A., & Naeem, A. (2015). Biodiesel production from low FFA waste cooking oil using heterogeneous catalyst derived from chicken bones. *Renewable Energy*, 76, 362–368. https://doi.org/10.1016/j.renene.2014.11.042.

Farouk, S. M., Tayeb, A. M., Abdel-Hamid, S. M. S., & Osman, R. M. (2024). Recent advances in transesterification for sustainable biodiesel production, challenges, and prospects: a comprehensive review. *Environmental science and pollution research international*, 31(9), 12722–12747. https://doi.org/10.1007/s11356-024-32027-4.

Fatimah, I.; Fadillah, G.; Sagadevan, S.; Oh, W.-C.; Ameta, K.L. (2023). Mesoporous silica-based catalysts for biodiesel production: a review. *ChemEngineering,* 7, 56. https://doi.org/10.3390/chemengineering7030056.

Fattahi, N., Triantafyllidis, K., Luque, R., & Ramazani, A. (2019). Zeolite-based catalysts: A valuable approach toward ester bond formation. *Catalysts*, 9(9). https://doi.org/10.3390/catal9090758.

Garcia, F. A. C., Araújo, D. R., Silva, J. C. M., De Macedo, J. L., Ghesti, G. F., Dias, S. C. L., Dias, J. A., & RFilho, G. N. (2011). Effect of cerium loading on structure and morphology of modified Ce-USY zeolites. *Journal of the Brazilian Chemical Society*, 22(10), 1894–1902. https://doi.org/10.1590/s0103-50532011001000010.

Ginting, S. B., Mufakhir, F. R., Santi, A. W., Astuti, W., Sumardi, S., Syarifuddin, H., Rohman, A., & Wibowo, Y. G. (2023). Cr(VI) removal from aqueous solution using modified zeolite-iron chloride and its future recommendation. *Inorganic Chemistry Communications,* 157, 111273. https://doi.org/10.1016/j.inoche.2023.111273.

Gonzaga, V. E., Romero, R., Gómez-Espinosa, R. M., Romero, A., Martínez, S. L., & Natividad, R. (2021). Biodiesel Production from Waste Cooking Oil Catalyzed by a Bifunctional Catalyst. *ACS Omega,* 6(37), 24092–24105. https://doi.org/10.1021/acsomega.1c03586.

Hadiyanto, H., Lestari, S. P., & Widayat, W. (2016). Preparation and Characterization of Anadara Granosa Shells and CaCO3 as Heterogeneous Catalyst for Biodiesel Production. *Bulletin of Chemical Reaction Engineering & Catalysis,* 11(1), 21-26. https://doi.org/10.9767/bcrec.11.1.402.21-26

Irwansyah, F. S., Amal, A. I., Diyanthi, E. W., Hadisantoso, E. P., Noviyanti, A. R., Eddy, D. R., & Risdiana, R. (2024). How to Read and Determine the Specific Surface Area of Inorganic Materials using the Brunauer-Emmett-Teller (BET) Method. *ASEAN Journal of Science and Engineering,* 4(1), 61–70. https://doi.org/10.17509/ajse.v4i1.60748.

Jian, X., Zhuang, X., Li, B., Xu, X., Wei, Z., Song, Y., & Jiang, E. (2018). Comparison of characterization and adsorption of biochars produced from hydrothermal carbonization and pyrolysis. *Environmental Technology & Innovation*, 10, 27–35. https://doi.org/10.1016/j.eti.2018.01.004.

Jumari, A., & Purwanto, A. (2013). Unjuk Kerja Katalis Heterogen Nanokomposit Zno/Fe2O3 Untuk Reaksi Transesterifikasi Pada Pembuatan Biodiesel Dari Minyak Jelantah Dengan Tinjauan Waktu Reaksi. *Ekuilibium,* 12(2), 35–39. https://doi.org/10.20961/ekuilibrium.v12i2.2178.

Kingkam, W., Nuchdang, S., Phalakornkule, C., Suwanmanee, U., & Rattanaphra, D. (2024). Synergistic effect of La2O3-Al2O3 based catalysts for efficient biodiesel production. *Journal of Industrial and Engineering Chemistry,* 143, 197-212 https://doi.org/10.1016/j.jiec.2024.08.023.

Kosuru, S. M. Y., Delhiwala, Y., Koorla, P. B., & Mekala, M. (2024). A review on the biodiesel production: Selection of catalyst, Pre-treatment, Post treatment methods. *Green Technologies and Sustainability,* 2(1), 100061. https://doi.org/10.1016/j.grets.2023.100061.

Kusumaningtyas, R. D., Prasetiawan, H., Anggraeni, N. D., Anisa, E. D. N., & Hartanto, D. (2023). Conversion of Free Fatty Acid in Calophyllum inophyllum Oil to Fatty Acid Ester as Precursor of Bio-Based Epoxy Plasticizer via SnCl2–Catalyzed Esterification. *Polymers*, 15(1), 123. https://doi.org/10.3390/polym15010123.

Leung, D. Y., Wu, X., & Leung, M. (2010). A review on biodiesel production using catalyzed transesterification. *Applied Energy,* 87(4), 1083–1095. https://doi.org/10.1016/j.apenergy.2009.10.006.

Li, J., Gao, M., Yan, W., & Yu J. (2023). Regulation of the Si/Al ratios and Al distributions of zeolites and their impact on properties. *Chemical Science,* 14, 1935. https://doi.org/10.1039/D2SC06010H.

Li, X., Zhu, J., Niu, S., Zheng, Y., & Xu, Y. (2025). Novel acid-base dual-activity heterogeneous Ba40-Ce15/ZSM-5 catalyst for biodiesel production: RSM-based optimization and performance analysis. *Energy,* 333, 137451. https://doi.org/10.1016/j.energy.2025.137451.

Lira, M. A., & Atadash, M. I. (2018). Effect of temperature variation on the production of biodiesel using neem oil. *International Journal of Research-GRANTHAALAYAH,* 6(9), 442–450. https://doi.org/10.29121/granthaalayah.v6.i9.2018.1267.

Maafa, I.M. (2022). Biodiesel synthesis from high free-fatty-acid Chicken fat using a scrap-dire Derived solid acid catalyst and KOH. *Polymers,* 14, 643. https://doi.org/10.3390/polym14030643

Malenga, E. N., Mulaba-Bafubiandi, A., & Nheta, W. (2022). Application of the response surface method (RSM) based on central composite design (CCD) and design space (DS) to optimize the flotation and the desliming conditions in the recovery of PGMs from mine sludge. *Separation Science and Technology*, 57(18), 2960–2983. https://doi.org/10.1080/01496395.2022.2092514.

Mazaheri, H., Ong, H. C., Amini, Z., Masjuki, H. H., Mofijur, M., Su, C. H., Badruddin, I. A., & Khan, T. Y. (2021). An overview of biodiesel production via calcium oxide based catalysts: Current state and perspective. *Energies,* 14(13), 3950. https://doi.org/10.3390/en14133950.

Mohammadi, M., Sabbaghi, S., Binazadeh, M., Ghaedi, S., & Rajabi, H. (2023). Type-1 α-Fe2O3/TiO2 photocatalytic degradation of tetracycline from wastewater using CCD-based RSM optimization. *Chemosphere,* 336,. https://doi.org/10.1016/j.chemosphere.2023.139311.

Momen, S. B., Siadat, S. D., Akbari, N., Ranjbar, B., & Khajeh, K. (2016). Applying central composite design and response surface methodology to optimize growth and biomass production of haemophilus influenzae type b. *Jundishapur Journal of Microbiology*, 9(6), 1–6. https://doi.org/10.5812/jjm.25246.

Monika, N., Banga, S., & Pathak, V. V. (2023). Biodiesel production from waste cooking oil: A comprehensive review on the application of heterogenous catalysts. *Energy Nexus,* 10, 100209. https://doi.org/10.1016/j.nexus.2023.100209.

Muhammad, Z., Garba, A., Ibrahim, Y., & Birniwa, A. H. (2024). Synthesis and characterization of zeolite sourced from rice husk lignocellulosic waste ash. *ChemSearch Journal,* 15(1), 80–85. https://www.ajol.info/index.php/csj/article/view/273648

Mulyatun, M., Prameswari, J., Istadi, I., & Widayat, W. (2022). Production of non-food feedstock based biodiesel using acid-base bifunctional heterogeneous catalysts: A review. *Fuel,* 314, 122749. https://doi.org/10.1016/j.fuel.2021.122749.

Munfarida, S., Widayat, Satriadi, H., Cahyono, B., Hadiyanto, Philia, J., & Prameswari, J. (2020). Geothermal industry waste-derived catalyst for enhanced biohydrogen production. *Chemosphere*, 258, 127274. https://doi.org/10.1016/j.chemosphere.2020.127274.

Naseef, H. H., & Tulaimat, R. H. (2025). Transesterification and esterification for biodiesel production: A comprehensive review

of catalysts and palm oil feedstocks. *Energy Conversion and Management X*, 26, 100931. https://doi.org/10.1016/j.ecmx.2025.100931.

Niawanti, H., & Zullaikah, S. (2018). Effect of extraction time on unreacted oil removal in biodiesel purification using deep eutectic solvent. *REAKTOR*, 18(2), 122. https://doi.org/10.14710/reaktor.18.2.122-127.

Okechukwu, O. D., Joseph, E., Nonso, U. C., & Kenechi, N. O. (2022). Improving heterogeneous catalysis for biodiesel production process. *Cleaner Chemical Engineering*, 3, 100038. https://doi.org/10.1016/j.clce.2022.100038.

Othman, A., Gowda, A., Andreescu, D., Hassan, M. H., Babu, S. V., Seo, J., & Andreescu, S. (2024). Two decades of ceria nanoparticle research: structure, properties and emerging applications. *Materials Horizons,* 11(14), 3213–3266. https://doi.org/10.1039/d4mh00055b

Rachmadona, N., Harada, Y., Amoah, J., Quayson, E., Aznury, M., Hama, S., Kondo, A., & Ogino, C. (2022). Integrated bioconversion process for biodiesel production utilizing waste from the palm oil industry. *Journal of Environmental Chemical Engineering*, 10(3), 107550. https://doi.org/10.1016/j.jece.2022.107550 .

Ramli, A., Farooq, M., Naeem, A., Khan, S., Hummayun, M., Iqbal, A., Ahmed, S., & Shah, L. A. (2017). Bifunctional Heterogeneous Catalysts for Biodiesel Production using Low Cost Feedstocks: A Future Perspective. *Frontiers in Bioenergy and Biofuels*, March. https://doi.org/10.5772/65553.

Roza, F. N., Widyaningrum, S. R., Alvita, L. R., & Rezki, A. S. (2025). Study of reaction temperature effects on the yield and quality of biodiesel synthesis from waste palm oil. *Indonesian Journal of Pure and Applied Chemistry,* 8(2), 45–53. https://doi.org/10.26418/indonesian.v8i2.96780.

Schlögl, R. (2015). Heterogeneous catalysis. *Angewandte Chemie International Edition*, 54(11), 3465–3520. https://doi.org/10.1002/anie.201410738.

Sharma, P., & Mohal, S. (2020). Parametric optimization of submerged arc welding process parameters by response surface methodology. *Materials Today Proceedings*, 24, 673–682. https://doi.org/10.1016/j.matpr.2020.04.321

Shobhana-Gnanaserkhar, N., Asikin-Mijan, N., AbdulKareem-Alsultan, G., Sivasangar-Seenivasagam, N., Izham, S. M., & Taufiq-Yap, Y. (2020). Biodiesel production via simultaneous esterification and transesterification of chicken fat oil by mesoporous sulfated Ce supported activated carbon. *Biomass and Bioenergy*, 141, 105714. https://doi.org/10.1016/j.biombioe.2020.105714.

Sumari, S., Arni, S., Santoso, A., Sholikah, L. P., Asrori, M. R., & Budianto, A. (2024). Contribution of Malang quartzite-based silica in K2O/zeolite Y catalyst for methyl ester synthesis of off grade crude palm oil. *Heliyon,* 10(13), e33563. https://doi.org/10.1016/j.heliyon.2024.e33563

Uche, C. U., Okezue, M. A., Amidu, I., & Byrn, S. R. (2024). Model adequacy in assessing the predictive performance of regression models in pharmaceutical product optimization: the bedaquiline solid lipid nanoparticle example. *Scientia Pharmaceutica*, 92(4), 64. https://doi.org/10.3390/scipharm92040064.

Widayat, N., Hadiyanto, N., Satriadi, H., Cahyono, B., Astuti, W. I. S. T., & Febrianti, P. (2019). Synthesis of Zeolite X Molecular Sieve from Geothermal Solid Waste. *Materials Today Proceedings*, 13, 137–142. https://doi.org/10.1016/j.matpr.2019.03.203.

Widayat, N., Satriadi, H., Setyojati, P. W., Shihab, D., Buchori, L., Hadiyanto, H., & Nurushofa, F. A. (2024). Preparation Cao/MgO/Fe3O4 magnetite catalyst and catalytic test for biodiesel production. *Results in Engineering*, 22, 102202. https://doi.org/10.1016/j.rineng.2024.102202.

Widiarti, N., Ni'mah, Y. L., Bahruji, H., & Prasetyoko, D. (2019). Development of CAO from natural calcite as a heterogeneous base catalyst in the formation of biodiesel: review. *Journal of Renewable Materials,* 7(10), 915–939. https://doi.org/10.32604/jrm.2019.07183.

Xie, W., & Wang, H. (2019). Immobilized polymeric sulfonated ionic liquid on core-shell structured Fe3O4/SiO2 composites: A magnetically recyclable catalyst for simultaneous transesterification and esterifications of low-cost oils to biodiesel. *Renewable Energy,* 145, 1709–1719. https://doi.org/10.1016/j.renene.2019.07.092.

Yaakouby, I. E., Borji, A., Ettalibi, O., Kouar, J., Abouliatim, Y., Hlaibi, M., & Kamil, N. (2025). One-pot conversion Allium sativum peels into a cost-effective carbon-based heterogeneous acid catalyst for renewable biodiesel production using palm oil refining by-products. *Energy Conversion and Management,* 327, 119551. https://doi.org/10.1016/j.enconman.2025.119551.

Yu, H., Sun, J., Chen, X., Wang, B., Liang, X., Gao, M., & Si, H. (2023). Synthesis of a novel acid-base bifunctional Zn/Ca–Zr catalyst for biodiesel application: Experimental and molecular simulation studies. *Renewable Energy*, 217, 119138. https://doi.org/10.1016/j.renene.2023.119138.

Yudiastuti, S. O. N., Handayani, W., Sari, E. K. N., Wijaya, R., Brilliantina, A., & Slamet, A. H. H. (2024). The utilization of trichoderma viride in optimising xylanase production from coffee cherry processing waste. *International Journal of Islamic Education Research and Multiculturalism (IJIERM),* 6(1), 102–122. https://doi.org/10.47006/ijierm.v6i1.298.

Yusof, A.M., Nizam, N.A. & Rashid, N.A.A. (2010). Hydrothermal conversion of rice husk ash to faujasite-types and NaA-type of zeolites. *J Porous Mater* 17, 39–47. https://doi.org/10.1007/s10934-009-9262-y.

Zhang, B., Gao, M., Geng, J., Cheng, Y., Wang, X., Wu, C., Wang, Q., Liu, S., & Cheung, S. M. (2021). Catalytic performance and deactivation mechanism of a one-step sulfonated carbon-based solid-acid catalyst in an esterification reaction. *Renewable Energy,* 164, 824–832. https://doi.org/10.1016/j.renene.2020.09.076.

Zhang, L., Albert Ng, T. C., Liua, X., Gua, Q., Panga, Y., & Zhanga, Z., *et al.* (2020). Hydrogenated TiO2 membrane with photocatalytically enhanced antifouling for ultrafiltration of surface water. *Applied Catalysis B: Environmental,* 264, 118528. https://doi.org/10.1016/j.apcatb.2019.118528.

Zhu, G., Graver, R., Emdadi, L., Liu, B., Choi, K. Y., & Liu, D. (2014). Synthesis of zeolite@metal–organic framework core–shell particles as bifunctional catalysts. *RSC Advances*, 4(58), 30673. https://doi.org/10.1039/c4ra03129f .